Pergamon

Int. J. Heat Mass Transfer. Vol. 40, No. 1, pp. 111–121, 1997

0017–9310/97 $15.00 + 0.00

PII: S0017–9310(96)00060–9

The effect of thermal stratification on natural convection in a vertical porous insulation layer

D. A. S. REES

School of Mechanical Engineering, University of Bath, Claverton Down, Bath BA2 7AY, U.K.

and

J. L. LAGE†

Mechanical Engineering Department, Southern Methodist University, Dallas, TX 75275-0337, U.S.A.

(*Received* 17 *April* 1995 *and in final form* 1 *February* 1996)

Abstract—We consider the two-dimensional free convection flow in a rectangular porous container where the impermeable bounding walls are held at a temperature which is a linearly decreasing function of height. Attention is focused on the case where the local temperature drop across the container is zero. Two cases are considered, namely, containers of finite aspect ratio and those of asymptotically large aspect ratio. For both cases it is found that modes bifurcate in pairs as the linear stability equations admit an infinite set of double eigenvalues. The weakly nonlinear evolution of the primary pair of eigenmodes is analysed, and it is found that the resulting steady-state flow is nonunique as the realized steady flow is dependent on the precise form of the initial disturbance. For asymptotically tall boxes the weakly nonlinear evolution of the pair of modes is governed by coupled pair of Burger-like equations. These are analyzed both numerically and using asymptotic methods. No evidence of persistently unsteady flow is found. Copyright © 1996 Elsevier Science Ltd.

1. INTRODUCTION

Natural convection in porous media is of practical interest in several science and engineering areas. For instance, the problem of heat and mass transport through fibrous insulation is not only of interest to the biologist studying the energy balance of mammals [1, 2], but also to the design engineer working on building insulation [3]. Other important application areas are those of geothermal energy systems [4–6] and geophysics (e.g. thawing subsea permafrost—Gosink and Baker [7] and magma chambers—Lowell [8]).

The simplest geometrical configuration of a fully saturated porous medium is that of a rectangular enclosure. The majority of existing archival publications consider steady and uniform boundary conditions. Some more complex conditions have been studied recently: spatially periodic heating [9–11], time periodic boundary conditions [12, 13], inclined thermal gradients [14, 15], and layering [16–18].

A classical thermal configuration which is relevant to the study of geothermal activities, underground transport of pollutants, paper processing, crystal growth, building insulation, and gas reservoirs, is that of heating from horizontal surfaces; this particular configuration is frequently treated as a stability problem. The determination of stability criteria is important because the transition from one mode of convection to another is accompanied by changes in the rates of heat and mass transport. The characterization of the subsequent supercritical regime is then fundamental for the control of thermal processes. The classical example of such a supercritical regime is the Horton–Rodgers–Lapwood natural convection flow within a horizontal fluid saturated porous medium layer heated from below or cooled from above [19, 20]. This is the porous medium analogue of Bénard convection in clear fluid systems, and it assumes a long enough horizontal layer such that the bounding vertical sidewalls do not affect the transport or stability phenomena.

It is worth mentioning that, for low permeability porous media, where the permeability is sufficiently low that Darcy's law is valid, the supercritical Horton–Rogers–Lapwood regime near but above criticality is characterized by a cellular flow. The convection regime can be simulated for different wavenumbers considering a finite horizontal layer with impermeable and adiabatic conditions imposed at the vertical boundaries. A review of linear stability analysis, weakly nonlinear theory, and numerical and experimental studies is presented in Chap. 6 of Nield and Bejan [20].

Finite enclosures heated from the horizontal and vertical surfaces are very important in thermal insulation design. Kassoy and Cotte [21] and Wang *et al.* [22] studied the convection effect of side-wall heat loss

† Author to whom correspondence should be addressed.

NOMENCLATURE

A, B weakly nonlinear amplitudes of modes A and B, respectively
b square root of the critical Rayleigh number
c_1, c_2, c_3, c_4 Landau constants in equation (17a)
d_1, d_2, d_3, d_4 Landau constants in equation (17b)
d half the dimensional channel width
f y-dependent part of the streamfunction perturbation
g y-dependent part of the temperature perturbation
$\hat{g}$ gravitational acceleration
G dimensional temperature gradient
H nondimensional height of the channel
k wavenumber
K permeability of the porous medium
m, n integers associated with different linear modes
p pressure
R Darcy–Rayleigh number
t time
T dimensional temperature
u, v Darcy velocities in the vertical and horizontal directions, respectively
x, y vertical and horizontal co-ordinates, respectively
X slow x-scale in weakly nonlinear analysis.

Greek symbols
β coefficient of thermal expansion
δ weakly nonlinear expansion parameter
ε weakly nonlinear expansion parameter
λ complex growth rate
θ temperature
Θ temperature perturbation
ψ streamfunction
Ψ streamfunction perturbation
κ thermal diffusivity of the saturated medium
σ heat capacity ratio of the medium to that of the fluid
μ viscosity of fluid
ρ density of fluid
τ slow timescale
ξ boundary layer x-coordinate.

Subscripts
0 reference value
t derivative with respect to t
x derivative with respect to x
y derivative with respect to y.

Superscript
$\tilde{}$ dimensional variable.

and of a conducting boundary in a small aspect ratio porous enclosure or vertical slot. Kimura and Bejan [23] studied the case of heating from the top and from the side. Their results showed that the convection driven by the horizontal temperature gradient persists, even when the vertical stabilizing gradient is larger than the horizontal gradient. More recently, Vadasz *et al.* [24] investigated the effect of perfectly conducting vertical surfaces (uniform and steady temperatures) on the natural convection in porous medium enclosure isothermally heated from below or from above. The conservation equations were solved numerically using a finite differences method for a fixed aspect ratio (length/height) equal to 2. They demonstrated that for this boundary configuration the system is conductively unstable, for a motionless solution is not possible, regardless of the magnitude and direction of the vertical temperature gradient.

The present work extends that of ref. [24] by considering the stability of a thermally-stratified fully saturated porous medium enclosure. The constant temperature of the vertical surfaces decreases linearly with the height of the enclosure from the temperature of the bottom surface to the temperature of the top surface. The linear stability analysis of the analogous clear fluid problem was investigated by Banks and Zaturska [25]. This model is an appropriate approximation of a system where the heat capacity of the solid vertical surfaces is much higher than that of the saturated medium. A thorough theoretical analysis is presented considering enclosures with finite aspect ratio and with asymptotically large aspect ratio (vertical slots).

2. FORMULATION OF THE PROBLEM

We consider the free convection flow in a rectangular porous container where the vertical sidewalls have identical linearly decreasing temperature profiles. The top and bottom surfaces are held at a constant temperature, respectively, equal to that of the adjoining sidewalls; these conditions ensure that the basic state consists of a linearly stratified temperature field and no flow. All four walls are assumed to be impermeable. The configuration is sketched in Fig. 1 and the detailed dimensional boundary conditions are given there.

The Darcy–Boussinesq equations governing two-dimensional free convection flow in an isotropic porous medium are given by

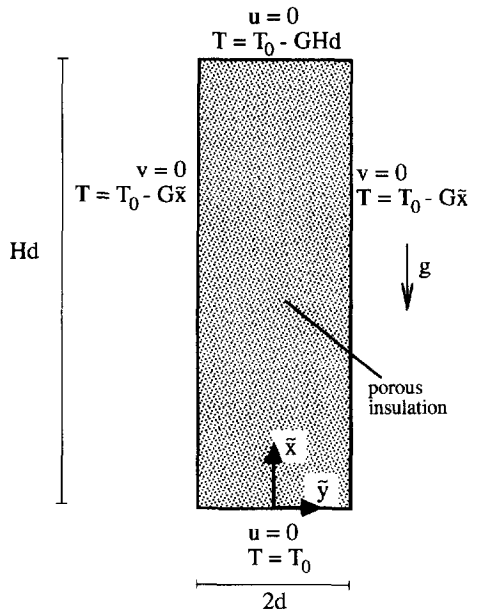

Fig. 1. Sketch of the flow domain and coordinate system.

$$\frac{\partial \tilde{u}}{\partial \tilde{x}} + \frac{\partial \tilde{v}}{\partial \tilde{y}} = 0 \tag{1a}$$

$$\tilde{u} = -\frac{K}{\mu}\frac{\partial \tilde{p}}{\partial \tilde{x}} + \frac{\rho \hat{\boldsymbol{g}} \beta K}{\mu}(T - T_0) \tag{1b}$$

$$\tilde{v} = -\frac{K}{\mu}\frac{\partial \tilde{p}}{\partial \tilde{y}} \tag{1c}$$

$$\sigma \frac{\partial T}{\partial \tilde{t}} + \tilde{u}\frac{\partial T}{\partial \tilde{x}} + \tilde{v}\frac{\partial T}{\partial \tilde{y}} = \kappa\left(\frac{\partial^2 T}{\partial \tilde{x}^2} + \frac{\partial^2 T}{\partial \tilde{y}^2}\right), \tag{1d}$$

where K is the permeability of the porous medium, μ is the dynamic viscosity, $\hat{\boldsymbol{g}}$ gravity, β the isobaric coefficient of volumetric thermal expansion, T_0 a reference temperature, κ the thermal diffusivity of the saturated medium, and σ the ratio of the heat capacity of the saturated medium to that of the fluid. The dependent variables, $\tilde{u}$, $\tilde{v}$, $\tilde{p}$ and T are the Darcy seepage velocities, pressure (static and dynamic, but not hydrostatic) and temperature, respectively. The coordinate, $\tilde{x}$, is measured in the upward vertical direction, while $\tilde{y}$ is the horizontal coordinate. Note also that for systems with small Darcy number and large Prandtl number, the Darcy model is expected to be reasonably accurate within the Rayleigh number range investigated here, as far as inertial effects are concerned [26].

The temperature of both bounding walls is set at $T = T_0 - G\tilde{x}$, where the constant G is a dimensional temperature gradient; we assume that G is positive in order to obtain an unstable thermal stratification of the fluid.

All the above variables are nondimensionalized by setting

$$t = \frac{\kappa}{d^2\sigma}\tilde{t} \quad (u, v) = \frac{d}{\kappa}(\tilde{u}, \tilde{v}) \tag{2a, b}$$

$$(x, y) = d^{-1}(\tilde{x}, \tilde{y}) \quad p = \frac{K}{\kappa\mu}\tilde{p} \tag{2c, d}$$

$$\theta = \frac{T - T_0}{Gd}. \tag{2e}$$

Equations (1a–d) become

$$\frac{\partial u}{\partial x} + \frac{\partial v}{\partial y} = 0. \tag{3a}$$

$$u = -\frac{\partial p}{\partial x} + R\theta \tag{3b}$$

$$v = -\frac{\partial p}{\partial y} \tag{3c}$$

$$\frac{\partial \theta}{\partial t} + u\frac{\partial \theta}{\partial x} + v\frac{\partial \theta}{\partial y} = \frac{\partial^2 \theta}{\partial x^2} + \frac{\partial^2 \theta}{\partial y^2} \tag{3d}$$

which are to be solved subject to the boundary conditions,

$$v = 0 \quad \theta = -x \quad \text{on } y = \pm 1 \tag{3e}$$

$$u = 0 \quad \theta = 0 \quad \text{on } x = 0 \tag{3f}$$

$$u = 0 \quad \theta = -H \quad \text{on } x = H, \tag{3g}$$

where H is the nondimensional height of the box containing the porous medium, d is the half-width of the box, and R is the Darcy–Rayleigh number based on the temperature gradient, G

$$R = \frac{\rho \hat{\boldsymbol{g}} \beta K G d^2}{\mu\kappa}. \tag{4}$$

Note that Hd is the dimensional height of the box.

We can eliminate the pressure in the usual way by introducing a streamfunction, ψ, according to

$$u = \frac{\partial \psi}{\partial y} \quad v = -\frac{\partial \psi}{\partial x}. \tag{5a, b}$$

Hence equations (3a–d) reduce to

$$\nabla^2 \psi = R\theta_y, \tag{6a}$$

$$\theta_t + \psi_y \theta_x - \psi_x \theta_y = \nabla^2 \theta; \tag{6b}$$

the boundary conditions for ψ are simply that $\psi = 0$ on all four boundaries, while the temperature conditions are given in equations (3e–g).

It is easily verified that

$$\psi = 0 \quad \theta = -x, \tag{7a, b}$$

is a solution of (6a) and (6b) for all values of R and H. The remainder of this paper is concerned with the linear stability of this conduction solution and its subsequent weakly nonlinear development.

3. LINEAR STABILITY ANALYSIS

We begin by considering the fate of small disturbances to the conduction profile. On setting $\psi = \Psi$ and $\theta = \Theta - x$ in equations (1) and (2), and linearizing the resulting equations, we obtain

$$\nabla^2\Psi = R\Theta_x \tag{8a}$$

$$\Theta_t = \nabla^2\Theta + \Psi_x. \tag{8b}$$

As both Ψ and Θ are zero on the top and bottom boundaries we can Fourier-decompose the disturbances in the x-direction by setting

$$\begin{pmatrix}\Psi\\ \Theta\end{pmatrix} = \begin{pmatrix}f(y)\\ g(y)\end{pmatrix} e^{\lambda t}\sin kx, \tag{9}$$

where λ is a complex growth rate, and the wavenumber, k, takes only those values which will enable the modes to satisfy the endwall boundary conditions, i.e. $k = n\pi/H$ for integer values of n. The functions f and g introduced in equation (9) satisfy the equations

$$f'' - k^2 f = Rg' \tag{10a}$$

$$\lambda g = g'' - k^2 g + f'. \tag{10b}$$

subject to $f(\pm 1) = g(\pm 1) = 0$. It is straightforward to show that the principle of exchange of stabilities holds and therefore that neutral stability is given by setting $\lambda = 0$. The resulting eigenvalue problem for R is satisfied by the pair of solutions,

$$\begin{aligned} f_1 &= 2\cos(\pi y/2)\cos(by/2)\\ g_1 &= -(2/b)\cos(\pi y/2)\sin(by/2) \end{aligned} \tag{11a}$$

$$\begin{aligned} f_2 &= -(2/b)\cos(\pi y/2)\sin(by/2)\\ g_2 &= -(2/b^2)\cos(\pi y/2)\cos(by/2), \end{aligned} \tag{11b}$$

where $b = R^{1/2}$ and $R = \pi^2 + 4k^2$ for *both* modes. These modes shall be referred to as modes A and B, respectively, and they have been normalized such that $g_1'(-1)$ and $f_2'(-1)$ are both equal to 1 in the limit $k \to 0$. It may also be shown that higher modes exist for which $R = m^2\pi^2 + 4k^2$ where both m and n are integers and where $k = n\pi/H$ again; these are similar in profile to those given explicitly in equation (11), and each ordered pair (m, n) has an associated pair of modes.

It is easily seen that R is minimized when $m = 1$ and we shall concentrate on this case, since $m = 1$ corresponds to the first pair modes to be destabilized as R increases. R is further minimized in the limit of an asymptotically tall container, that is as $H \to \infty$ or $k \to 0$. In this regard the present flow is similar to the analogous clear fluid problem [25] and to the horizontal porous Bénard problem with insulated horizontal surfaces (cf. Nield and Bejan [20] p. 147). However, k is not a parameter which can be varied continuously, for it is related to the height of the container. Indeed, for a given height, H, we shall consider only the $n = 1$ value of k given above (i.e. $k = \pi/H$), for this provides the minimum value of R for any given container.

4. WEAKLY NONLINEAR ANALYSIS FOR FINITE CONTAINERS

Given a container of finite aspect ratio, that is, one for which H is neither asymptotically small nor large, we consider weakly nonlinear convection by expanding ψ and θ in the form,

$$\psi = \varepsilon\psi_1 + \varepsilon^2\psi_2 + \varepsilon^3\psi_3 + \cdots \tag{12a}$$

$$\theta = -x + \varepsilon\theta_1 + \varepsilon^2\theta_2 + \varepsilon^3\theta_3 + \cdots \tag{12b}$$

$$R = R_0 + \varepsilon^2 R_2 + \cdots, \tag{13}$$

where $R_0 = \pi^2 + 4k^2$ is the critical Rayleigh number, and equation (13) defines the small parameter, ε, where $R_2 = O(1)$ as $\varepsilon \to 0$. It is appropriate to define a slow timescale, τ, where $\tau = \varepsilon^2 t$.

At $O(\varepsilon)$ in the expansion the equations governing ψ_1 and θ_1 are identical in form to equation (6). Hence, we take

$$\begin{pmatrix}\psi_1\\ \theta_1\end{pmatrix} = A(\tau)\begin{pmatrix}f_1(y)\\ g_1(y)\end{pmatrix}\sin kx + B(\tau)\begin{pmatrix}f_2(y)\\ g_2(y)\end{pmatrix}\sin kx, \tag{14}$$

where (f_1, g_1) and (f_2, g_2) are given by equations (11a) and (11b), respectively.

At $O(\varepsilon^2)$ we obtain

$$\nabla^2\psi_2 = R_0\theta_{2y}, \tag{15a}$$

$$\nabla^2\theta_2 + \psi_{2y} = \psi_{1y}\theta_{1x} - \psi_{1x}\theta_{1y}, \tag{15b}$$

for which the solution is

$$\psi_2 = \frac{\pi}{8}(A^2 + B^2)\sin\pi y\sin 2kx, \tag{16a}$$

$$\theta_2 = -\tfrac{1}{8}(A^2 + B^2)(1 + \cos\pi y)\sin 2kx. \tag{16b}$$

At $O(\varepsilon^3)$ we obtain a pair of equations for ψ_3 and θ_3 in which the inhomogeneous terms contain components proportional to one or the other of the $O(\varepsilon)$ eigensolutions given in equations (11a, b). On following the usual solvability condition procedure these equations have solutions only if the following pair of Landau equations are satisfied:

$$c_1 A_\tau = c_2 R_2 A - c_3 A^3 - c_4 A B^2 \tag{17a}$$

$$d_1 B_\tau = d_2 R_2 B - d_3 B^3 - d_4 A^2 B, \tag{17b}$$

where the coefficients, c_i, d_i, $i = 1, \ldots, 4$, are given by

$$\begin{aligned} c_1 &= 2[1 + (\pi^2/4kb)\sin b] \quad c_2 = 1\\ c_3 &= 3R_0/16 \quad c_4 = 3/16\\ d_1 &= \frac{2}{R_0}[1 - (\pi^2/4kb)\sin b] \quad d_2 = 1/R_0\\ d_3 &= 3/16 \quad d_4 = 3/(16R_0). \end{aligned} \tag{18}$$

It may be shown that there are an infinite number of steady-state solutions for A and B, and these take the form

$$A^2 = \frac{16R_2\alpha}{3R_0} \quad B^2 = \frac{16R_2(1-\alpha)}{3}, \tag{19}$$

where α can take any value between 0 and 1, inclusive. A linear stability analysis of solution (19) for an *arbitrary* value of α yields one decaying mode and one neutrally stable mode, and hence all the solutions given by equation (19) are neutrally stable. Thus, the degeneracy found at leading order with the appearance of a double eigenvalue has not been removed at third-order: there is no preferred weakly nonlinear solution and the solution obtained depends on the form of the initial disturbance. Such a result arises as a direct consequence of the fact that $c_3d_3 = c_4d_4$ in the Landau equations, above. The conclusion is, therefore, that the final steady-state solution is highly dependent on the form of the initial disturbance. Preliminary work on the numerical solution of the full governing equations, (1) and (2), confirms the persistence of nonuniqueness into the strongly nonlinear regime—we intend to report on this elsewhere.

It is necessary to mention that, although the final steady flow in the weakly nonlinear Bénard and porous Bénard problems is also dependent on the initial disturbance, it is always composed of one roll mode, rather than as an arbitrary sum of two distinct modes which is the case here. Some degeneracy always exists in such finite horizontal layer problems, because the wavenumber and orientation of the roll depends on the precise form of the disturbance, and the final steady solution is also neutrally stable. For these latter problems $c_3d_3 > c_4d_4$ which ensures that a single mode steady solution is obtained. When $c_3d_3 < c_4d_4$ the final steady solution has a square or rectangular planform (see Riahi [27], Rees and Riley [18]) and is therefore composed of a definite, rather than an arbitrary, pair of modes.

5. WEAKLY NONLINEAR ANALYSIS FOR ASYMPTOTICALLY TALL CONTAINERS

An asymptotically tall container corresponds to an asymptotically small value of the wavenumber, k. We therefore rescale the x-coordinate using $X = kx$ and use k as the small parameter in a weakly nonlinear analysis. The slow timescale is now given by $\tau = k^2t$, and, in terms of X, the container lies between $X = 0$ and $X = \pi$. The full governing equations become

$$k^2\psi_{XX} - \psi_{yy} = R\theta_y \tag{20a}$$

$$k^2\theta_\tau + k(\psi_y\theta_X - \psi_X\theta_y) = k^2\theta_{XX} + \theta_{yy}, \tag{20b}$$

where $k \ll 1$. The weakly nonlinear expansion has the form

$$\psi = k\psi_1 + k^2\psi_2 + k^3\psi_3 + \cdots \tag{21a}$$

$$\theta = -x + k\theta_1 + k^2\theta_2 + k^3\theta_3 + \cdots \tag{21b}$$

$$R = R_0 + k^2R_2 + \cdots. \tag{21c}$$

At $O(k)$ in the expansion we have

$$\psi_{1yy} = \pi^2\theta_{1y} \tag{22a}$$

$$\theta_{1yy} + \psi_{1y} = 0, \tag{22b}$$

for which the solution is taken to be

$$\begin{pmatrix}\psi_1\\ \theta_1\end{pmatrix} = A(X,\tau)\begin{pmatrix}(1+\cos\pi y)\\ -(\sin\pi y)/\pi\end{pmatrix} + B(X,\tau)\begin{pmatrix}-(\sin\pi y)/\pi\\ -(1+\cos\pi y)/\pi^2\end{pmatrix}; \tag{23}$$

the y-dependent parts of this solution are identical to the respective small k limits of the solutions given in equation (14).

The $O(k^2)$ solutions are simply $\psi_2 = 0$ and $\theta_2 = 0$ as the equations are homogeneous. At $O(k^3)$ we obtain the pair of equations,

$$\psi_{3yy} - \pi^2\theta_{3y} = R_2\theta_{1y} - \psi_{1XX}, \tag{24a}$$

$$\theta_{3yy} + \psi_{3y} = \theta_{1\tau} - \theta_{1XX} + \psi_{1y}\theta_{1X} - \psi_{1X}\theta_{1y}, \tag{24b}$$

where the right hand sides contain components proportional to the $O(k)$ eigensolutions. Insisting that these equations have a solution yields the following pair of amplitude equations:

$$A_\tau = R_2A + 4A_{XX} + A_XB - AB_X, \tag{25a}$$

$$B_\tau = \tfrac{1}{3}R_2B + \tfrac{4}{3}B_{XX} - \pi^2AA_X - BB_X; \tag{25b}$$

these are to be solved subject to the boundary conditions

$$A = B = 0 \quad \text{on } X = 0 \quad \text{and} \quad X = \pi. \tag{25c}$$

A straightforward linear stability analysis of the solution, $A = 0$, $B = 0$, shows that the eigensolutions, $A \propto \sin X$, $B = 0$ and $A = 0$, $B \propto \sin X$ both bifurcate at $R_2 = 4$, a result which is consistent with the form of the neutral curve, $R = \pi^2 + 4k^2$, and the expansion (21c).

5.1. *Analysis for small values of* $(R_2 - 4)$

Consider now the behaviour of the solutions of equation (25) in the near neighbourhood of $R_2 = 4$ by setting

$$A = \delta A_1 + \delta^2A_2 + \delta^3A_3 + \cdots \tag{26a}$$

$$B = \delta B_1 + \delta^2B_2 + \delta^3B_3 + \cdots \tag{26b}$$

$$R_2 = 4 + \delta^2S + \cdots \tag{26c}$$

$$\tau = \delta^2\hat{\tau} \tag{26d}$$

and

$$A_1 = \hat{A}(\hat{\tau}) \quad B_1 = \hat{B}(\hat{\tau}) \tag{26e}$$

in equations (25). The expansion parameter, δ, is

taken to be small. Omitting details of the weakly nonlinear analysis we find that a solvability condition at $O(\delta^3)$ yields the amplitude equations

$$\hat{A}_{\hat{t}} = S\hat{A} - \tfrac{3}{16}(\pi^2\hat{A}^2 + \hat{B}^2)\hat{A} \tag{27a}$$

$$\hat{B}_{\hat{t}} = S\hat{B} - \tfrac{3}{16}(\pi^2\hat{A}^2 + \hat{B}^2)\hat{B}. \tag{27b}$$

The coefficients in these equations are identical to the small-k limit of the corresponding coefficients in equations (17a, b). Therefore we have an asymptotic matching between this case and the $k = O(1)$ case and hence, all the results found there are also applicable here, including the fact that steady solutions are nonunique and neutrally stable.

5.2. *Analysis for large values of* R_2

Before we present fully numerical results for intermediate values of R_2, we turn our attention to very large values of R_2, for it is possible to obtain strongly nonlinear results when the container is asymptotically tall.

The pure-B solution is the easier case to discuss and therefore we shall consider this solution first. Setting $A = 0$ in equation (25) gives

$$(R_2 - 3B_X)B + 4B_{XX} = 0, \tag{28}$$

an equation which is closely related to Burger's equation. The boundary conditions are that $B(0) = 0$ and $B(\pi) = 0$. It is easy to verify that

$$B = \tfrac{1}{3}R_2(X - X_0), \tag{29}$$

where X_0 is arbitrary, is a solution of equation (28), but it does not satisfy the boundary conditions. We can choose a value of X_0 to satisfy only one of the boundary conditions and it is necessary to perform a singular perturbation analysis to enable the second condition to be satisfied. Choosing $X_0 = \pi$ gives

$$B = \tfrac{1}{3}R_2(X - \pi), \tag{30}$$

means that the condition at $X = \pi$ is satisfied, but not that at $X = 0$. It may be shown that for large values of R_2 a thin layer of thickness $O(R_2^{-1})$ near $X = 0$ enables the $X = 0$ boundary condition to be satisfied. If we rescale the X-coordinate using

$$X = R_2^{-1}\xi, \tag{31}$$

expand B as

$$B = R_2 B_0 + B_1 + O(R_2^{-1}), \tag{32}$$

and use standard techniques of matched asymptotic analysis, it is possible to show that

$$B_0 = -\frac{\pi}{3}\tanh\frac{\pi\xi}{8} \tag{33a}$$

and

$$B_1 = \frac{1}{3}\left[\frac{8}{\pi}\tanh\frac{\pi\xi}{8}\left(\ln\cosh\frac{\pi\xi}{8} - \frac{1}{2}\right) + \frac{\xi}{2}\operatorname{sech}^2\frac{\pi\xi}{8} + \operatorname{sech}^2\frac{\pi\xi}{8}\int_0^{\xi}\ln\cosh\frac{\pi\eta}{8}\,d\eta\right] + (4 + 8\ln 2)\left[\frac{1}{\pi}\tanh\frac{\pi\eta}{8} + \frac{\xi}{2}\operatorname{sech}^2\frac{\pi\eta}{8}\right]. \tag{33b}$$

Given equations (33a, b) it is easy to verify that equation (32) takes the form

$$B \sim -\frac{\pi}{3} + \frac{\xi}{3}R_2^{-1} \quad \text{as } R_2 \to \infty, \tag{34}$$

which, when written in terms of X, is identical to equation (30).

An almost identical analysis is obtained if the boundary condition at $X = 0$ is satisfied first by choosing $X_0 = \pi$—in this case a boundary layer of the same $O(R_2^{-1})$ thickness is formed at $X = \pi$.

When we take X_0 equal to neither 0 nor π then mixed modes are obtained. It is easily verified that

$$B \sim \tfrac{1}{3}R_2(X - X_0), \tag{35a}$$

and

$$A \sim 0 \tag{35b}$$

over almost the whole of the range $0 \leqslant X \leqslant \pi$ for large values of R_2. At $X = 0$ and $X = \pi$ thin layers occur which may be analysed using a virtually identical analysis to that given above. However, a third thin layer, an internal layer, occurs near where $X = X_0$. It may be shown using a scaling argument that it has an $O(R_2^{-1/2})$ thickness, and hence we rescale according to

$$A = R_2^{-1/2}\bar{A},\ B = R_2^{-1/2}\bar{B}, \quad \text{and} \quad X = X_0 + R_2^{-1/2}\bar{X}. \tag{36}$$

The steady forms of equations (25a, b) now become

$$\bar{A} + 4\bar{A}_{\bar{X}\bar{X}} + \bar{A}_{\bar{X}}\bar{B} - \bar{A}\bar{B}_{\bar{X}} = 0, \tag{37a}$$

$$\bar{B} + 4\bar{B}_{\bar{X}\bar{X}} + 3\pi^2\bar{A}\bar{A}_{\bar{X}} - 3\bar{B}\bar{B}_{\bar{X}} = 0, \tag{37b}$$

and these have to be solved subject to the matching conditions that $\bar{A} \to 0$ and $\bar{B}_{\bar{X}} \to \frac{1}{3}$ as $\bar{X} \to \pm\infty$. This system has an infinite number of solutions which are identical in profile, but invariant under a Gallilean transformation or origin-shift; such nonuniqueness arises from an $O(R_2^{-1/2})$ uncertainty in the location of X_0. Therefore we set $\bar{B} = 0$ at $\bar{X} = 0$ in order to obtain a unique solution. It is simple to confirm that $\bar{B}$ is antisymmetric and $\bar{A}$ is symmetric about the origin, and therefore we can solve this problem from $\bar{X} = 0$ to $\bar{X} = \infty$ using $\bar{A}_{\bar{X}}(0) = 0$ as the extra boundary condition. The profiles were obtained as the final steady state of an unsteady calculation using a slightly modified version of the numerical code described below.

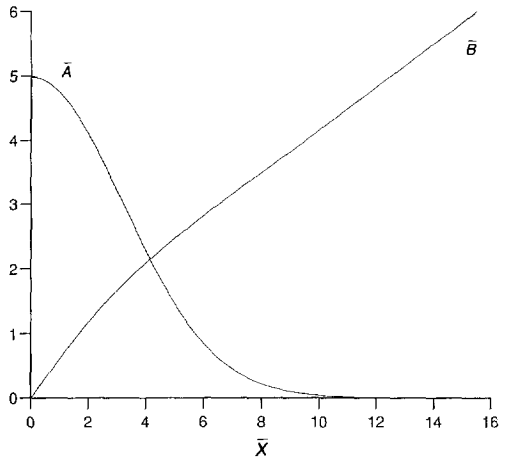

Fig. 2. Internal layer mixed-mode profiles for asymptotically large values of R_2.

This *unique* solution is presented in Fig. 2, and it can be compared with fully numerical solutions of equations (25a, b) below. A different way of viewing the effect of this internal layer may be seen in Fig. 3

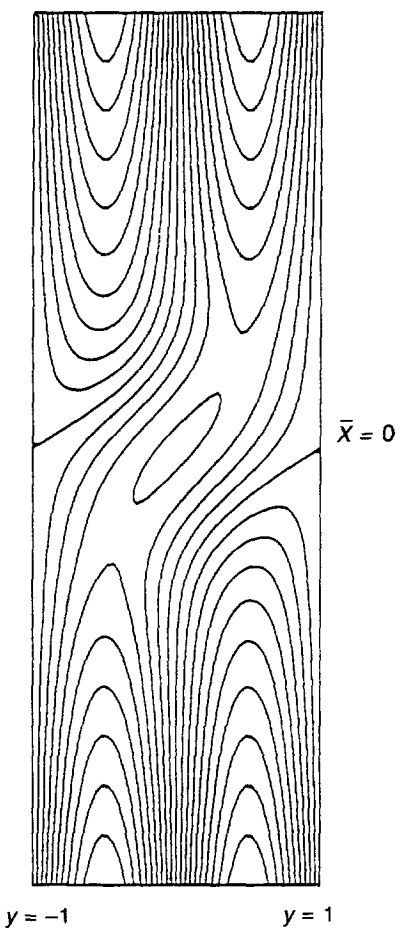

Fig. 3. Representative streamlines near the internal layer for asymptotically large values of R_2. Note the aspect ratio of the container is also asymptotically large.

which shows streamlines corresponding to the profiles given in Fig. 2. The streamfunction is given by

$$\psi \sim kR_2^{-1/2}[-(1+\cos \pi y)\bar{A}(\bar{X}) + (\sin \pi y/\pi)\bar{B}(\bar{X})]. \tag{38}$$

In viewing this figure (and also Figs. 6 and 8) it is important to be reminded of the fact that the container is asymptotically tall and hence, the $\bar{X}$ and y scales represented there are very different in magnitude. Far from $\bar{X} = 0$ the flow exhibits a two-cell structure, but near $\bar{X} = 0$ the dividing streamline in the centre of the cavity attaches itself to one of the vertical walls thereby allowing one of the cells to occupy the whole of the width of the cavity, at least locally. The streamline pattern obtained possesses centro-symmetry about $\bar{X} = 0$ and $y = 0$. Therefore the mixed-mode is composed of three cells, two of which occupy only half the length of the cavity, and the other the full length of the cavity. The full-length cell expands in width near $\bar{X} = 0$ and changes side from left to right, or *vice versa*. This behaviour is also seen in the computations for intermediate values of R_2 given below.

5.3. *Intermediate values of* R_2

When R_2 is neither asymptotically large nor asymptotically close to 4, it is necessary to solve the unsteady equations numerically. We have used the DuFort–Frankel method which is second-order accurate in both space and time. All the computations presented here are based on either 100 or 200 equally spaced intervals lying between $X = 0$ and $X = \pi$. Numerical stability limits the choice of the timestep and this becomes increasingly restrictive as R_2 becomes large. It became quite evident that when the timestep is sufficiently small to avoid numerical divergence, but still remains too large, then spuriously time-periodic solutions are obtained. However, reducing the timestep further allows the solution to tend to a steady state. In fact, all the cases we considered tend towards a steady solution if the timestep is sufficiently small, and no evidence of persistently unsteady behaviour was found.

Figure 4 shows the steady B-mode solution for various values of R_2. When R_2 is close to 4 the profiles resemble the sinusoidal form given in equation (23). As R_2 increases, the profile becomes increasingly asymmetric. At large values of R_2 it becomes linear over most of the channel and displays a distinct boundary layer structure at $X = \pi$, in confirmation of the analysis presented in Section 5.2. The negative counterpart to these solutions is given by $-B(\pi - X)$. where $B(X)$ is displayed in Fig. 4.

Mixed modes are displayed in Fig. 5. Here we have specified the initial conditions to be such that the steady A-profile is symmetric and the B-profile antisymmetric. When R_2 is close to 4 the profiles are again sinusoidal, but as R_2 becomes increasingly large the A-profile is concentrated increasingly at $X = \pi/2$ which is where $B = 0$, and the B-profile develops two boundary

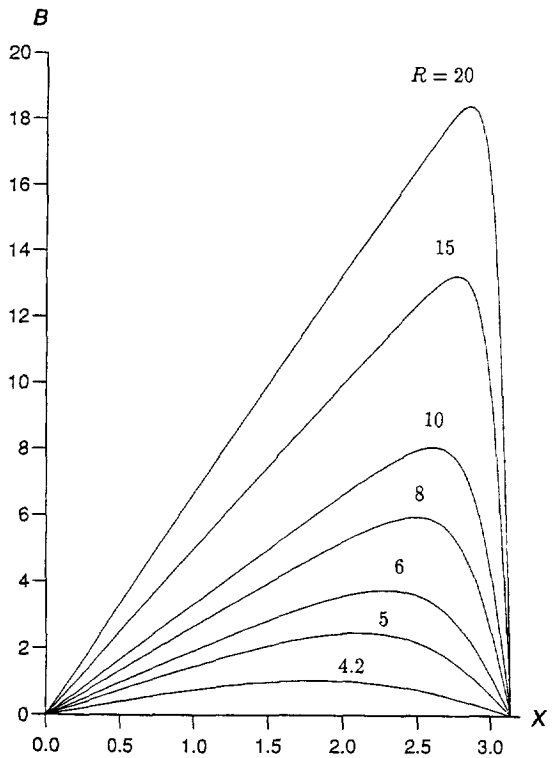

Fig. 4. Pure B-mode profiles for various values of R_2.

layers and one internal layer, in agreement with the analysis of Section 5.2. The profiles for $R_2 = 100$ should be compared with the (half-range) asymptotic profiles given in Fig. 2, Streamline plots corresponding to Fig. 5 are shown in Fig. 6. When the Rayleigh number is very close to the critical value the flow is predominantly unicellular, with two very thin recirculation regions at diametrically opposed corners of the box. As the Rayleigh number is increased, the recirculating regions increase in size until both occupy approximately a quarter of the container. At this stage the flow pattern is virtually identical to that of the asymptotic solution displayed in Fig. 3. The two boundary layers at either end are very clearly displayed and the internal layer at the centre is evident.

Figure 7 shows various steady solutions for $R_2 = 100$ in order to demonstrate that nonuniqueness is also a feature of even strongly nonlinear solutions of equation (25) and shows the existence of the three thin layers. These solutions were generated by specifying a range of different initial conditions and allowing the code to run until the steady state was attained. Of particular interest is the variation in the location of the A-profile when $R_2 = 100$. The amplitude of the A-mode is substantially different from zero only over a narrow range of values of X—this range corresponds to where B is close to zero, thereby providing a qualitative confirmation of the asymptotic theory of the internal layer given in Section 5.2. Again, to clarify, we present streamline plots of some of the solutions given in Fig. 7—these are shown in Fig. 8. The location of the region where the B-mode is zero corresponds to where the streamlines emerge from the sidewalls; at these locations the flow pattern is again very similar to that shown in Fig. 3, even though the value of R used is not particularly large.

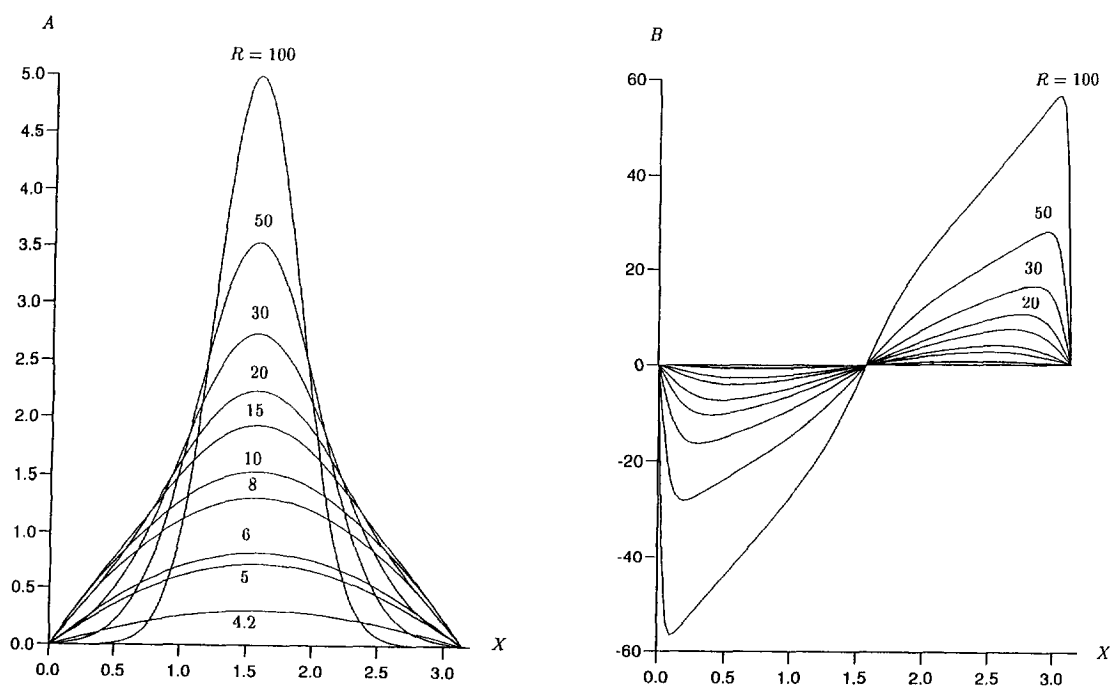

Fig. 5. Mixed-mode profiles for various values of R_2.

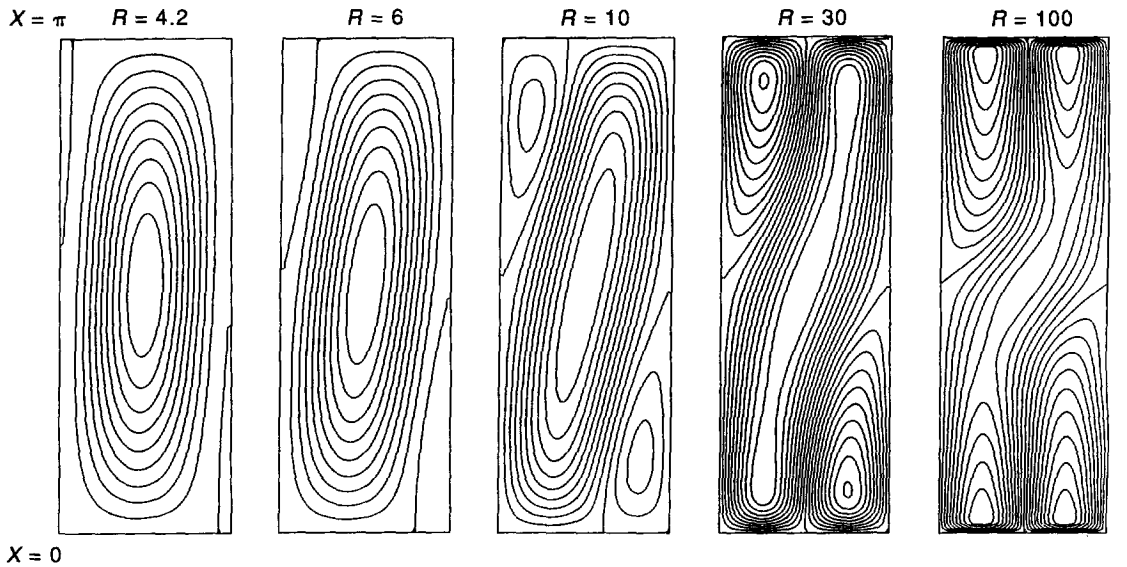

Fig. 6. Representative streamlines corresponding to the profiles given in Fig. 5.

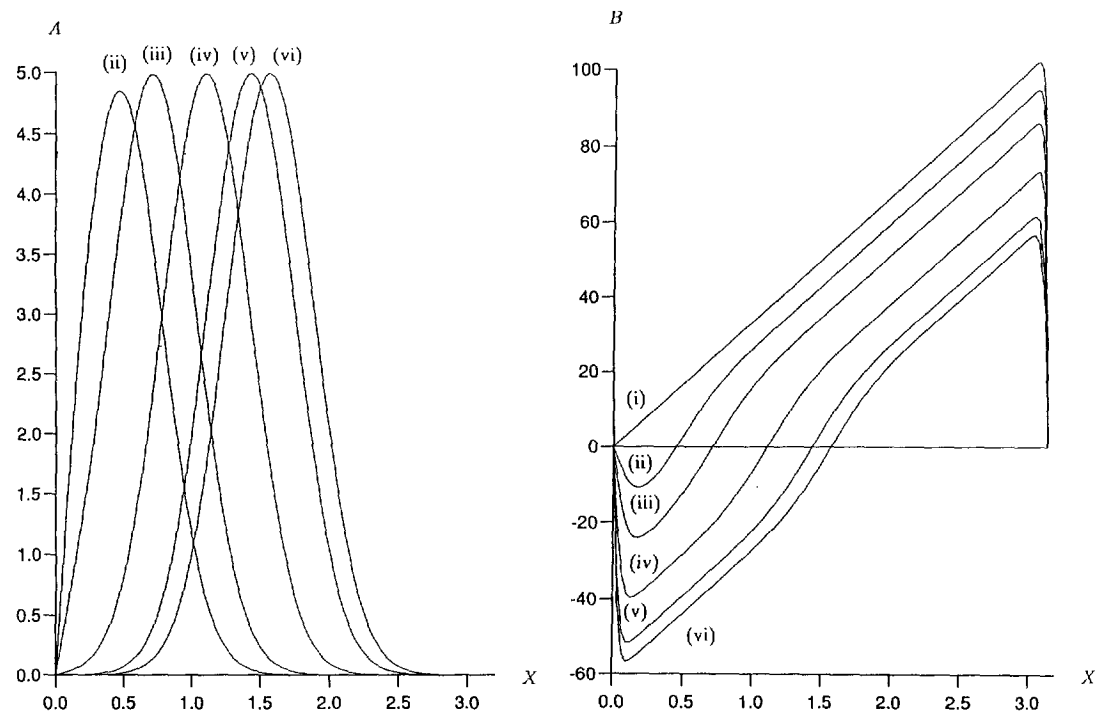

Fig. 7. Different steady-state mixed-mode profiles for $R_2 = 100$ demonstrating the presence of nonunique solutions. These profiles were obtained by setting $A = a \sin X$ and $B = b \sin X$ as initial profiles where (i) $a = 0, b = 1$, (ii) $a = 1, b = 50$, (iii) $a = 1, b = 30$, (iv) $a = 1, b = 15$, (v) $a = 1, b = 5$, (vi) $a = 1, b = 0$.

6. CONCLUSIONS AND DISCUSSION

In this paper we have sought to analyse the linear instability and the subsequent weakly nonlinear evolution of disturbances in an unstably stratified vertical porous container. It was found that unstable modes bifurcate in pairs, because the linearized instability equations admit an infinite set of double eigenvalues. The subsequent weakly nonlinear evolution of the primary pair of modes was analysed and it was found that the resulting steady state is nonunique, and is in fact highly dependent on the precise form of the initiating disturbances. When the container is asymptotically tall and the Rayleigh number sufficiently high the B-mode profile develops either a single boundary layer structure or a three-layer structure, one of which is an internal layer. In the former case the A-mode is

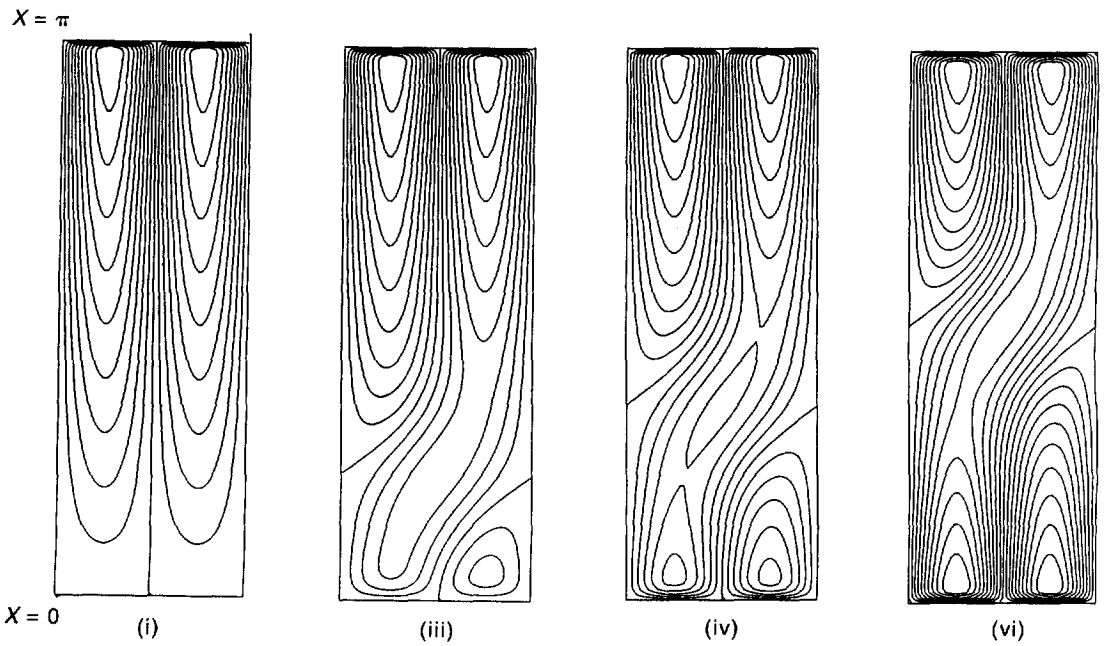

Fig. 8. Representative streamlines corresponding to some of the profiles given in Fig. 7.

absent, but in the latter case A is nonzero only where the B-profile is close to zero at an internal layer. The internal and boundary layers have different asymptotic thicknesses.

It is necessary to comment further on the nonuniqueness of the weakly nonlinear solutions. Many other free convection problems have a degenerate linearized eigenvalue problem associated with them in the sense that linear modes are nonunique. In the Bénard problem, for example, there is only one mode *shape*, but the phase and orientation are indeterminate if the layer is infinite in horizontal extent. Here, though, we have two entirely different mode shapes at onset and this is a very different form of degeneracy. It is somewhat surprising that the present weakly nonlinear analysis does not result in one particular combination of the two modes being preferred over all the others, but that there are an infinite number of combinations of the two modes which are realizable. Even in the Bénard problem with sidewalls, where the fluid is contained in a cuboid of such a size that an exact number of linearized modes fits into it in either direction, two linearized modes are possible, but a weakly nonlinear analysis will give either one or the other as being preferred, depending on the aspect ratio of the box. Even if the horizontal cross-section is square, the resulting convection pattern is drawn from a small finite number of competing patterns. Mathematically, the difference between these qualitatively different scenarios lies in the values of Landau coefficients of the nonlinear terms.

We intend to extend this work in various directions. In this paper we have assumed that the flow is two-dimensional and it is necessary to investigate whether or not three-dimensional effects are more important in a channel of infinite spanwise extent. Even if three-dimensional effects turn out to be more important in layers of infinite spanwise extent, the present analysis will still apply for containers where the spanwise width is such that three-dimensional modes are subdominant. This will always be true for sufficiently narrow layers. Further, it is also important to investigate in detail the flow in the strongly nonlinear regime, especially from the point of view of determining when the flow becomes unsteady. The work of Gill [28] on the differentially heated vertical channel with uniform wall temperatures shows that the basic flow in this configuration is stable. We should also like to analyse the transition between Gill's flow and the one considered here by studying the effects of both differential heating and nonuniform wall temperatures; in effect this will be a consideration of the effect of an inclined thermal gradient in a vertical channel.

Acknowledgements—The authors are thankful to the organisers of the 1994 Heat Transfer Workshop held in Bucharest, Romania, for fomenting the initiation of our research collaboration. Professor Lage is grateful for the financial support provided by the J. L. Embrey Professorship in Mechanical Engineering.

REFERENCES

1. J. L. Lage and A. Bejan, Natural convection from a vertical surface covered with hair, *Int. J. Heat Fluid Flow* **12**, 46–53 (1991).
2. W.-J. Yang and N. Zhang, Introducing the next generation in insulation. In *Transport Phenomena in Thermal Engineering*, Vol. 2 (Edited by J. S. Lee, S. H. Chung and K. Y. Kim), pp. 1489–1493. Begell House, New York, (1993).
3. C. J. Simonson, Y.-X. Tao and R. W. Besant, Thermal

hysteresis in fibrous insulation, *Int. J. Heat Mass Transfer* **36,** 4433–4441 (1993).
4. P. Cheng, Heat transfer in geothermal systems, *Adv. Heat Transfer* **14,** 1–104 (1978).
5. P. Cheng, Geothermal heat transfer. In *Handbook of Heat Transfer Applications* (Edited by W. M. Rohsenow, J. P. Hartnett and E. N. Ganić) (2nd Edn.) McGraw-Hill, New York (1985).
6. A. Hadim and L. C. Burmeister, Conceptual design of a downward-convecting solar pond filled with a water-saturated porous medium, *ASME J. Solar Energy Engng* **114,** 240–245 (1992).
7. J. P. Gosink and G. C. Baker, Salt fingering in subsea permafrost: some stability and energy considerations, *J. Geophys. Res.* **95,** 9575–9583 (1990).
8. R. P. Lowell, Double diffusive convection in partially molten silicate systems: its role during magma production and in magma chambers, *J. Volcanol. Geotherm. Res.* **26,** 1–24 (1985).
9. D. A. S. Rees, The effect of long-wavelength thermal modulations on the onset of convection in an infinite porous layer heated from below, *Q. J. Mech. Appl. Math.* **43,** 189–214 (1990).
10. D. A. S. Rees and D. S. Riley, The effects of boundary imperfections on convection in a saturated porous layer: non-resonant wavelength excitation, *Proc. R. Soc. London. A* **421,** 303–339 (1989).
11. D. A. S. Rees and D. S. Riley, The effects of boundary imperfections on convection in a saturated porous layer: near-resonant wavelength excitation, *J. Fluid Mech.* **199,** 133–154 (1989).
12. M. Kazmierczak and A. Muley, Steady and transient natural convection experiments in a horizontal porous layer: the effects of a thin top fluid layer and oscillating bottom wall temperature, *Int. J. Heat Fluid Flow* **15,** 30–41 (1994).
13. B. Antohe and J. L. Lage, A dynamic thermal insulator: inducing resonance within a fluid saturated porous medium enclosure heated periodically from the side, *Int. J. Heat Mass Transfer* **37,** 751–782 (1994).
14. D. A. Nield, Convection in a porous medium with inclined temperature gradient, *Int. J. Heat Mass Transfer* **34,** 87–92 (1991).
15. D. M. Manole and J. L. Lage, Numerical simulation of supercritical Hadley circulation, induced by inclined temperature gradients, within a porous medium layer, *Int. J. Heat Mass Transfer* **38,** 2583–2594 (1995).
16. R. McKibbin and M. J. O'Sullivan, Onset of convection in a layered porous medium heated from below, *J. Fluid Mech.* **96,** 375–393 (1980).
17. R. McKibbin and M. J. O'Sullivan, Heat transfer in a layered porous medium heated from below, *J. Fluid Mech.* **111,** 141–173 (1981).
18. D. A. S. Rees and D. S. Riley, The three-dimensional stability of finite-amplitude convection in a layered porous medium heated from below, *J. Fluid Mech.* **211,** 437–461 (1990).
19. C. W. Horton and F. T. Rodgers, Convection currents in a porous medium, *J. Appl. Phys.* **16,** 367–370 (1945).
20. D. A. Nield and A. Bejan, *Convection in Porous Media.* Springer, Berlin (1992).
21. D. R. Kassoy and B. Cotte, The effects of sidewall heat loss on convection in a saturated porous vertical slot, *J. Fluid Mech.* **152,** 361–378 (1985).
22. M. Wang, D. R. Kassoy and P. D. Weidman, Onset of convection in a vertical slab of saturated porous media between two impermeable conducting blocks, *Int. J. Heat Mass Transfer* **30,** 1331–1341 (1987).
23. S. Kimura and A. Bejan, Natural convection in a stably heated corner filled with porous medium, *J. Heat Transfer* **107,** 293–298 (1985).
24. P. Vadasz, C. Braester and J. Bear, The effect of perfectly conducting side walls on natural convection in porous media, *Int. J. Heat Mass Transfer* **36,** 1159–1170 (1993).
25. W. H. H. Banks and M. B. Zaturska, Buoyancy-driven flow between parallel plane vertical walls, *J. Engng Math.* **25,** 375–397 (1991).
26. J. L. Lage, Effect of the convective inertia term on Bénard convection in a porous medium, *Numer. Heat Transfer A* **22,** 469–485 (1992).
27. D. N. Riahi, Nonlinear convection in a porous layer with finite conducting boundaries, *J. Fluid Mech.* **129,** 153–171 (1983).
28. A. E. Gill, A proof that convection in a porous vertical slab is stable, *J. Fluid Mech.* **35,** 545–547 (1969).